Signal degradation through module pins in VLSI packaging

by Ching-Chao Huang
Leon L. Wu

This paper investigates chip-to-chip communication through the modules and board in VLSI packaging. Transmission line models and frequency-dependent transmission line parameters are used in finding the frequency response. The time-domain solution is then obtained through the inverse Fast Fourier Transform. The results show that uncoated module pins, even of relatively short length, can cause severe signal degradation because of their magnetic property. The signal behavior is improved dramatically, however, when the module pins are coated with nonmagnetic conductive material.

Introduction

The thermal stress caused by the heat dissipation of bipolar integrated circuit chips makes it necessary to match the thermal coefficients of pins attached to the substrate. Many nickel–iron alloys (e.g., Kovar and Invar) have low expansion coefficients and are good candidates for use as module pins. However, with relative permeability ranging up to several thousands [1], the magnetic property of such alloys can have an adverse effect on signal propagation. The following study shows that the magnetic module pins, even though of relatively short length, can cause severe signal degradation in chip-to-chip communication. Dramatic improvements are obtained, however, when the pins are coated with even a very thin layer of good nonmagnetic conductor.

©**Copyright** 1987 by International Business Machines Corporation. Copying in printed form for private use is permitted without payment of royalty provided that (1) each reproduction is done without alteration and (2) the *Journal* reference and IBM copyright notice are included on the first page. The title and abstract, but no other portions, of this paper may be copied or distributed royalty free without further permission by computer-based and other information-service systems. Permission to *republish* any other portion of this paper must be obtained from the Editor.

Analysis

• *Model*

Figure 1 shows an example of a VLSI package in which the integrated circuit chips are mounted on the modules, and the modules are, in turn, mounted on the board. The signal path from one chip to another through the module(1)–pin(2)–board(3)–pin(4)–module(5) connection is now modeled by five sections of transmission lines, as shown in **Figure 2.** The driver in Chip A is represented by an ideal voltage source in series with a resistor R_S (= 10 ohms). A terminator R_L (= 50 ohms) is placed in front of a receiver in Chip B to reduce the signal reflection from a receiver (note that the receiver has a high input impedance). To single out the effect of the pins, it is assumed that ideal 50-ohm lines are achieved in both the modules and the board. The propagation constants are different, however, in that different materials, ceramic (with dielectric constant $\varepsilon_r = 9.5$) and epoxy glass ($\varepsilon_r = 4.5$), are used for the modules and the board, respectively.

The voltage at the receiver, V_o, is now solved in the frequency domain first. The voltage V_i and current I_i (i = 1–5) in each transmission line can be represented by the following [2]:

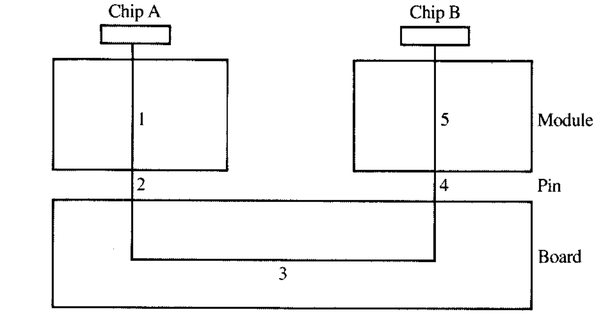

Figure 1

Chip-to-chip communication through the modules and board.

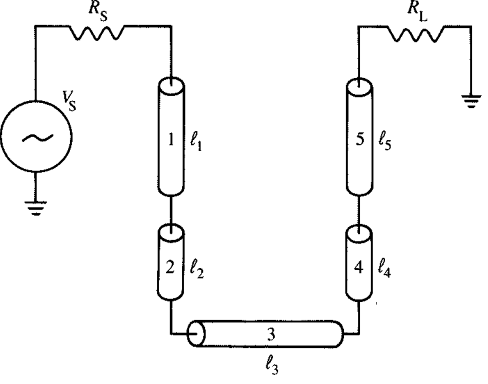

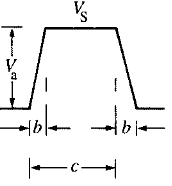

Figure 2

Model of the signal path in Figure 1. Here, $\ell_1 = \ell_3 = \ell_5 = 5$ cm, $\ell_2 = \ell_4 = 85$ mils; $R_S = 10$ ohms, $R_L = 50$ ohms; $V_a = 1.044$ volt, $b = 250$ ps, $c = 10$ ns.

$$V_i(z) = V_i^+ e^{-\gamma_i z} + V_i^- e^{+\gamma_i z}, \quad (1)$$

$$I_i(z) = Y_{ci}\,(V_i^+ e^{-\gamma_i z} - V_i^- e^{+\gamma_i z}), \quad (2)$$

where

$$Y_{ci} = 0.02 \text{ mho} \qquad \text{for } i = 1, 3, 5, \quad (3a)$$

$$= \sqrt{(G_{\text{eff}} + j\omega C_{\text{eff}})/(R_{\text{eff}} + j\omega L_{\text{eff}})} \qquad \text{for } i = 2, 4, \quad (3b)$$

$$e\gamma_i = j\omega\,\sqrt{\varepsilon_{ri}}/c_o \qquad \text{for } i = 1, 3, 5, \quad (4a)$$

$$= \sqrt{(R_{\text{eff}} + j\omega L_{\text{eff}})(G_{\text{eff}} + j\omega C_{\text{eff}})} \qquad \text{for } i = 2, 4, \quad (4b)$$

and $0 \leqq z \leqq \ell_i$; $\varepsilon_{r1,5} = 9.5$, $\varepsilon_{r3} = 4.5$; c_o is the speed of light. The transmission line parameters (R_{eff}, L_{eff}, G_{eff}, C_{eff}) for the pin regions are discussed in the next section.

By matching the boundary conditions at each interface between transmission lines, one has (see Appendix A)

$$[A][V] = [V_Q], \quad (5)$$

where $[A] = [a_{ij}]_{10\times10}$, $[V]^T = [V_1^+, V_1^-, \cdots, V_5^+, V_5^-]_{1\times10}$, and $[V_Q]^T = [V_S, 0, 0, \cdots, 0]_{1\times10}$; T denotes the transpose of the matrix. V_S is the Fourier transform of the source voltage. For a trapezoidal waveshape $V_S(t)$, as shown in Figure 2, $V_S(\omega)$ is as follows:

$$V_S(\omega) = V_a c\,\frac{\sin(\omega b/2)}{\omega b/2}\,\frac{\sin(\omega c/2)}{\omega c/2}\,e^{-j\omega(b+c)/2}. \quad (6)$$

In the following, we let $b = 250$ ps, $c = 10$ ns, and $V_a = 1.044$ volt. After one finds V_5^+ and V_5^-, the output voltage, V_o, is simply given by

$$V_o(\omega) = V_5(\ell_5) = V_5^+ e^{-\gamma_5 \ell_5} + V_5^- e^{+\gamma_5 \ell_5}. \quad (7)$$

The frequency response is then transformed to the time domain using the inverse Fast Fourier Transform (FFT) algorithm.

- *R, L, G, C of the module pins*

Uncoated case

The module pins are now modeled by finite circular cylinders, as shown in **Figure 3.** By neglecting the radiation resistance, the impedance per unit length, $Z(= R + j\omega L)$, of a finite circular cylinder can be written as

$$Z = Z_{\text{int}} + j\omega L_{\text{ext}}, \quad (8)$$

where Z_{int} and L_{ext} are the internal impedance and external inductance, respectively, and are given by [3, 4]

$$Z^*_{\text{int}} = R_{\text{int}} - j\omega L_{\text{int}} = \frac{\zeta}{2\pi a\sigma}\,\frac{J_o(\zeta a)}{J_1(\zeta a)}, \quad (9)$$

$$L_{\text{ext}} = \frac{\mu_o}{2\pi}\left(\ln\frac{2\ell}{a} - 1\right), \quad (10)$$

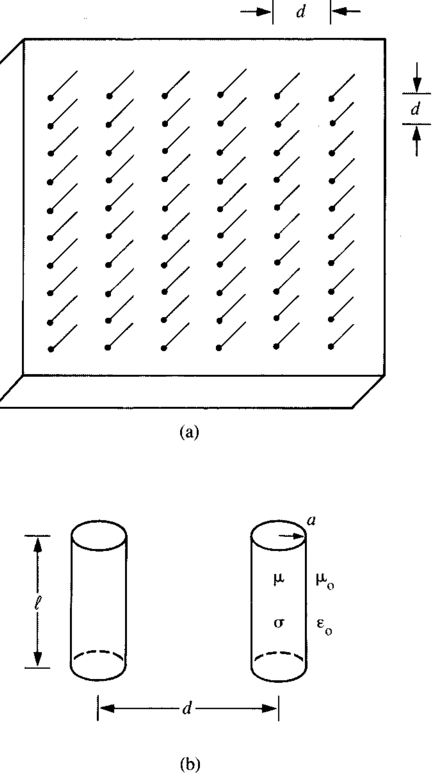

Figure 3

Module pins modeled by finite circular cylinders.

where $\zeta = \sqrt{j\omega\mu\sigma}$; $Z^*_{\rm int}$ denotes the complex conjugate of $Z_{\rm int}$, and $J_n(\cdot)$ is the nth order of Bessel's function. Note that Equation (10) is actually a low-frequency formula, which is independent of frequency. The total self-inductance $L(= L_{\rm int} + L_{\rm ext})$ per unit length can also be written in the following form [4]:

$$L = \frac{\mu_o}{2\pi}\left(\ln\frac{2\ell}{a} - 1\right) + \frac{\mu}{8\pi}\,T, \qquad (11)$$

where $0 \leqq T \leqq 1$; $T = 1$ at low frequency, and

$$T \approx 2\delta_S/a \qquad (12)$$

at high frequency. Here, δ_S $(= \sqrt{2/\omega\mu\sigma})$ is the skin depth.

The effect of the conductor's permeability on the mutual inductance is small, and the mutual inductance per unit length, M, between the module pins is calculated through the following [4]:

$$M = \frac{\mu_o}{2\pi}\left[\ln\left(\frac{\ell}{d} + \sqrt{1 + \frac{\ell^2}{d^2}}\right) - \sqrt{1 + \frac{d^2}{\ell^2}} + \frac{d}{\ell}\right]. \qquad (13)$$

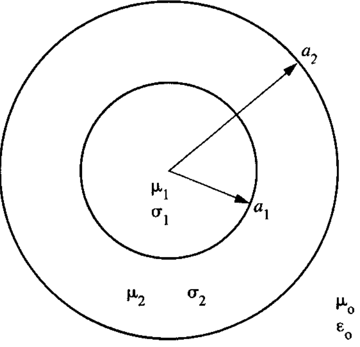

Figure 4

Cross section of a coated circular cylinder.

Coated case

For a coated cylinder, as shown in **Figure 4,** $Z^*_{\rm int}$ in Equation (9) is now replaced by

$$Z^*_{\rm int} = \frac{\zeta_2}{2\pi a_2\sigma_2}\,\frac{J_o(\zeta_2 a_2)}{J_1(\zeta_2 a_2)}\,B, \qquad (14)$$

where

$$B = \frac{1 - D\,\dfrac{N_o(\zeta_2 a_2)}{J_o(\zeta_2 a_2)}}{1 - D\,\dfrac{N_1(\zeta_2 a_2)}{J_1(\zeta_2 a_2)}} \qquad (15)$$

and

$$D = \frac{J_o(\zeta_2 a_1)J_1(\zeta_1 a_1) - \dfrac{\mu_1\zeta_2}{\mu_2\zeta_1}\,J_o(\zeta_1 a_1)J_1(\zeta_2 a_1)}{N_o(\zeta_2 a_1)J_1(\zeta_1 a_1) - \dfrac{\mu_1\zeta_2}{\mu_2\zeta_1}J_o(\zeta_1 a_1)N_1(\zeta_2 a_1)}. \qquad (16)$$

Here, $\zeta_1 = \sqrt{j\omega\mu_1\sigma_1}$, $\zeta_2 = \sqrt{j\omega\mu_2\sigma_2}$, and $N_n(\cdot)$ is the nth order of Neumann's function. Equations (10) and (13) can still be used to calculate $L_{\rm ext}$ and M except that a is replaced by a_2.

Figure 5(a–c) shows the calculated $R_{\rm int}$, $L_{\rm int}$, and $\omega L_{\rm int}$ for both coated and uncoated circular cylinders.

R_{eff}, L_{eff}, G_{eff}, C_{eff} in the pin regions

The module pins are assigned to carry both power and signal. Power pins are usually distributed uniformly to minimize cross talk between signal pins. **Figure 6(a)** shows a typical configuration with a ratio of one signal to one power pin. To examine the signal degradation through a pin, we

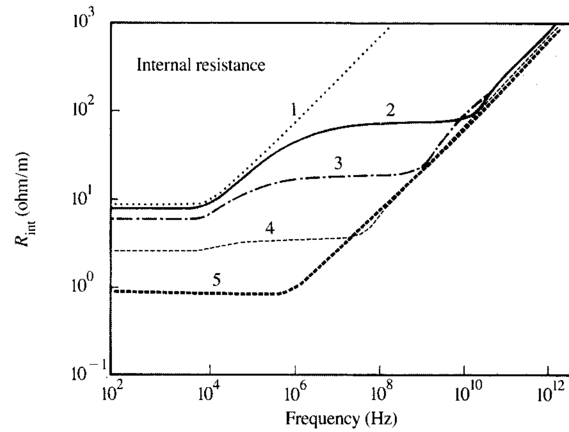

(a)

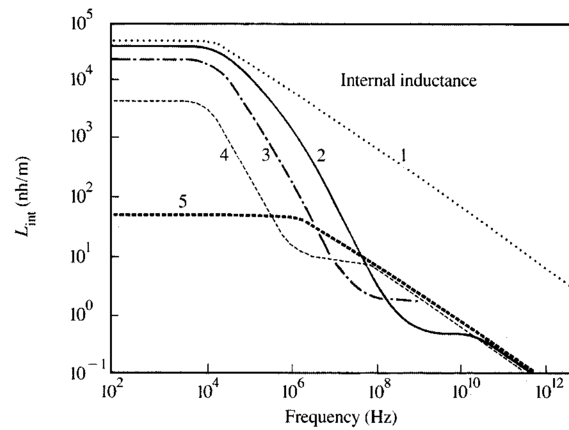

(b)

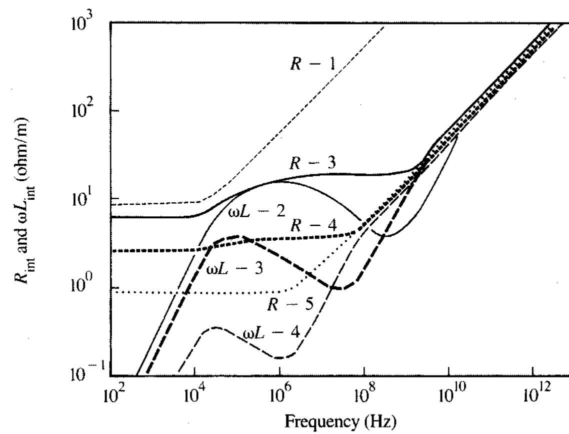

(c)

Figure 5

(a) R_{int}, (b) L_{int}, and (c) R_{int} and ωL_{int} of coated and uncoated circular cylinders: 1—solid Invar (a = 6.80 mils); 2—Invar (a_1 = 6.75 mils) + Pd coating ($a_2 - a_1$ = 0.05 mil); 3—Invar (a_1 = 6.75 mils) + Pd coating ($a_2 - a_1$ = 0.20 mil); 4—Invar (a_1 = 6.75 mils) + Pd coating ($a_2 - a_1$ = 1 mil); 5—solid Pd (a = 7.75 mils). μ/μ_0 = 1000 is assumed for Invar.

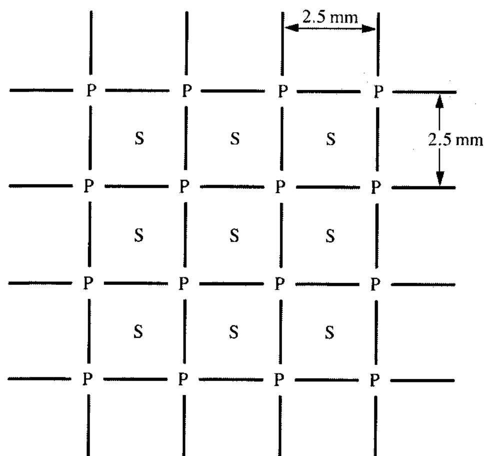

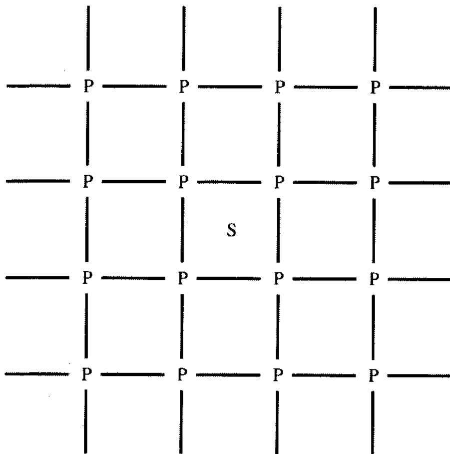

Figure 6

Signal (S)–power (P) pin pattern.

retain only one signal pin and try to include as many power pins as possible for the ground reference. Thus, the pin array for studying the signal degradation is now reduced to that of **Figure 6(b). Figure** 7 shows the circuit equivalent (without capacitance) of Figure 6(b), where the power pins are shorted together at both ends. For a two-port system, as in Figure 7, the following equation can be derived:

$$[\tilde{Z}][\tilde{I}] = [\tilde{V}_Q], \tag{17a}$$

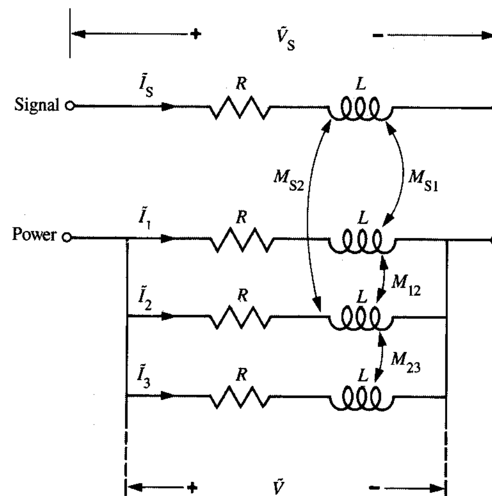

Figure 7

Partial circuit representation (without capacitance) of module pins.

$$\begin{bmatrix} R + j\omega L & j\omega M_{S1} & j\omega M_{S2} & \cdots & j\omega M_{SN} \\ j\omega M_{S1} & R + j\omega L & j\omega M_{12} & \cdots & j\omega M_{1N} \\ j\omega M_{S2} & j\omega M_{12} & R + j\omega L & \cdots & j\omega M_{2N} \\ \cdots & \cdots & \cdots & \cdots & \cdots \\ j\omega M_{SN} & j\omega M_{1N} & j\omega M_{2N} & \cdots & R + j\omega L \end{bmatrix} \tag{17b}$$

and

$$[\tilde{I}] = [\tilde{I}_S, \tilde{I}_1, \tilde{I}_2, \cdots, \tilde{I}_N]^T_{1\times(N+1)}, \tag{17c}$$

$$[\tilde{V}_Q] = [\tilde{V}_S, \tilde{V}, \tilde{V}, \cdots, \tilde{V}]^T_{1\times(N+1)}, \tag{17d}$$

In turn, Equations (17a–d) can be reduced to the following (see Appendix B):

$$\begin{bmatrix} Z_{11} & Z_{12} \\ Z_{12} & Z_{22} \end{bmatrix} \begin{bmatrix} \tilde{I}_S \\ \sum_{n=1}^{N} \tilde{I}_n \end{bmatrix} = \begin{bmatrix} \tilde{V}_S \\ \tilde{V} \end{bmatrix}. \tag{18}$$

Note that $\tilde{I}_S = -\sum_{n=1}^{N} \tilde{I}_n$. The effective impedance, Z_{eff} $(= R_{eff} + j\omega L_{eff})$, of the pin region is then given by

$$Z_{eff} = Z_{11} + Z_{22} - 2Z_{12}. \tag{19}$$

Assuming a TEM mode propagation in the air medium, C_{eff} is then given by

$$C_{eff} = \frac{\mu_0 \varepsilon_0}{L_{eff}} \bigg|_{\omega\to\infty}. \tag{20}$$

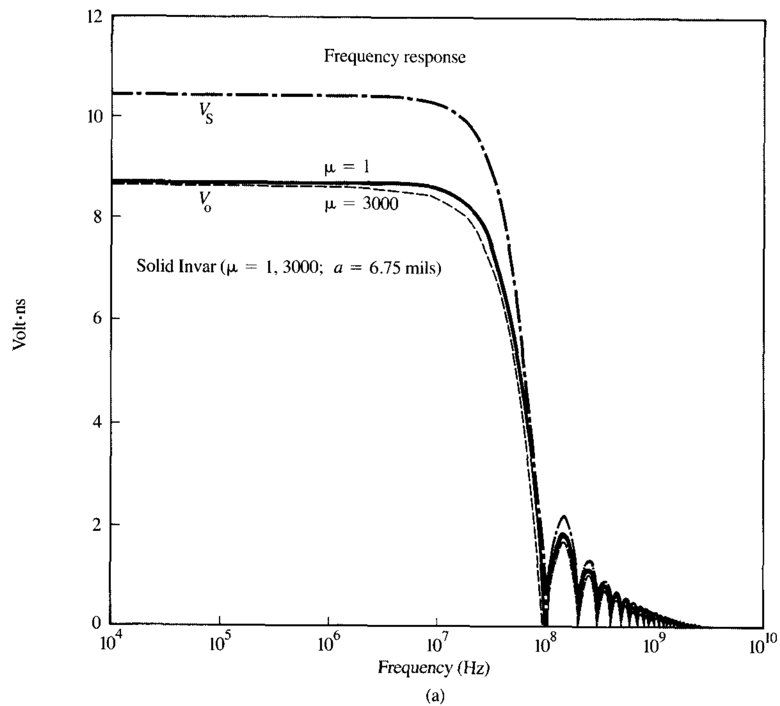

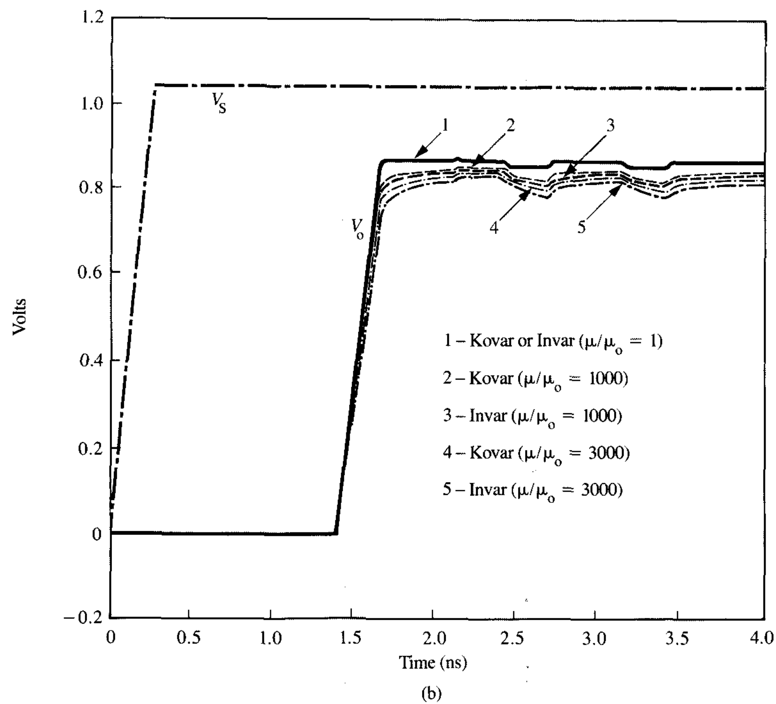

Figure 8

(a) Frequency and (b) time response of V_o where solid Invar and Kovar pins (a = 6.75 mils) are used, respectively.

Note that as $\omega \to \infty$, $L_{int} \to 0$, $L \approx L_{ext}$, and $R \ll \omega L$. Also, the air medium is assumed to be lossless, and thus $G_{eff} = 0$.

Table 1 shows an example of the calculated L_{eff} as a function of frequency and the number of power pins included. The power pins are chosen to be located symmetrically around the signal pin in a square pattern. The signal to power current ratios are also shown for comparison. Apparently, the lower the frequency, the more power pins must be included to get high accuracy. Here, L_{eff} at f = 5 MHz is of interest because it is the lowest harmonic that we used in the inverse FFT (the frequency response is sampled every 5 MHz). Besides the harmonics, a dc value is required in the inverse FFT. Note that at dc an infinite number of power pins (or, more realistically, all power pins in a module) should be included because the ground return current will flow uniformly through all power pins. Fortunately, the above procedures need not be followed at dc because as $\omega \to 0$, $R_{eff} \to R$ and $\omega L_{eff} \ll R_{eff}$, and V_o is simply given by

$$V_o(\omega = 0) \approx V_a c \frac{R_L}{R_S + R_L + 2R}. \tag{21}$$

Except at dc, all the results shown in the following section were calculated with 16 power pins included.

Results

Figure 8 shows the frequency and time response of V_o when solid Invar (σ = 1.215 mho/μm) and Kovar (σ = 2.041 mho/μm), respectively [1], are used for the module pins (a = 6.75 mils). The frequency response, sampled at 5 MHz, was converted to the time response using a 16 384-point inverse FFT algorithm. Generally speaking, more attenuation and slower rise time are observed as μ is increased. In a high-speed computer package environment, false switching and excessive delay have to be avoided [5]. The seemingly extra dc voltage drop for larger μ in Figure 8, actually caused by the RC delay, can make the receiver more susceptible to noise. The voltage dip, caused by the reflection from the impedance mismatch between the pins and the modules/board, in conjunction with the coupled noise and delta-I noise [5], if large enough, may penetrate the receiver's threshold band and make it false-switch. One observes that the signal degradation in Figure 8 is less dependent on μ when the more conductive material is used. Thus, when uncoated, the more conductive Kovar will be better than Invar electrically. In fact, if a perfect conductor ($\sigma \to \infty$) were used, μ would have no effect on the signal response at all. [One may note in Equation (8) that, as $\sigma \to \infty$, $Z \approx j\omega L_{ext}$.]

Figure 9 shows the signal behavior when the Invar module pins are coated with 0.2 mil of Pd (σ = 9.259 mho/μm). One observes that the signal response is improved dramatically when the pins are coated with even a thin layer of nonmagnetic conductor ($\mu = \mu_o$). The difference in the resultant signal response becomes negligible when both Kovar and Invar pins are suitably coated. Thus, one may choose freely between coated Kovar and coated Invar pins, so far as the electrical design is concerned. **Figure 10** shows the result with 0.01 mil of Pd plating, just to illustrate that an extremely thin layer of coating, which is not common, may not be good enough.

Table 1 L_{eff} vs. number of power pins (solid Invar pins are assumed, with a = 6.75 mils, ℓ = 85 mils, and μ/μ_o = 1).

No. of power pins	*Frequency* (MHz)	*Current ratio**	L_{eff} (μh/m)
4	5	1:0.25:0.25	0.452
	∞	1:0.25:0.25	0.390
16	5	1:0.1275:0.03940	0.4286
	∞	1:0.1538:0.02665	0.369
36	5	1:0.1199:0.01296	0.42773
	∞	1:0.1466:0.00842	0.3674
64	5	1:0.1189:0.00563	0.42771
	∞	1:0.1452:0.00341	0.36703
100	5	1:0.1186:0.00273	0.427726
	∞	1:0.1447:0.00157	0.366895

*Current ratio = signal current: maximum power current: minimum power current.

Conclusions

This paper has studied signal behavior in chip-to-chip communication due to the discontinuity of the module pins. The module pins, made of nickel–iron alloy (either Kovar or Invar), are of concern because of their magnetic property. In this analysis, the frequency-dependent transmission line parameters in the pin regions are calculated analytically for both uncoated and coated cases. The effect of the number of power pins to be included as the ground reference was also demonstrated. The signal response was illustrated in both the frequency and time domains. It was shown that the severe signal degradation due to the magnetic module pins can be eliminated by even a thin coating of good nonmagnetic conductor. That the signal response becomes relatively insensitive to the inner conductor's magnetic property (μ) can be understood, because at low frequency, R is independent of μ, and $R \gg \omega L$, while at high frequency, R is mostly due to the outer layer, and $L \approx L_{ext}$, which is also independent of μ. Finally, it is noted that μ has been assumed to be a frequency-independent constant in the foregoing analysis. A worst-case scenario was attempted in that μ was chosen deliberately large in the calculation. The complex permeability as a function of frequency and magnetic field strength can be easily included in the analysis when such information is available.

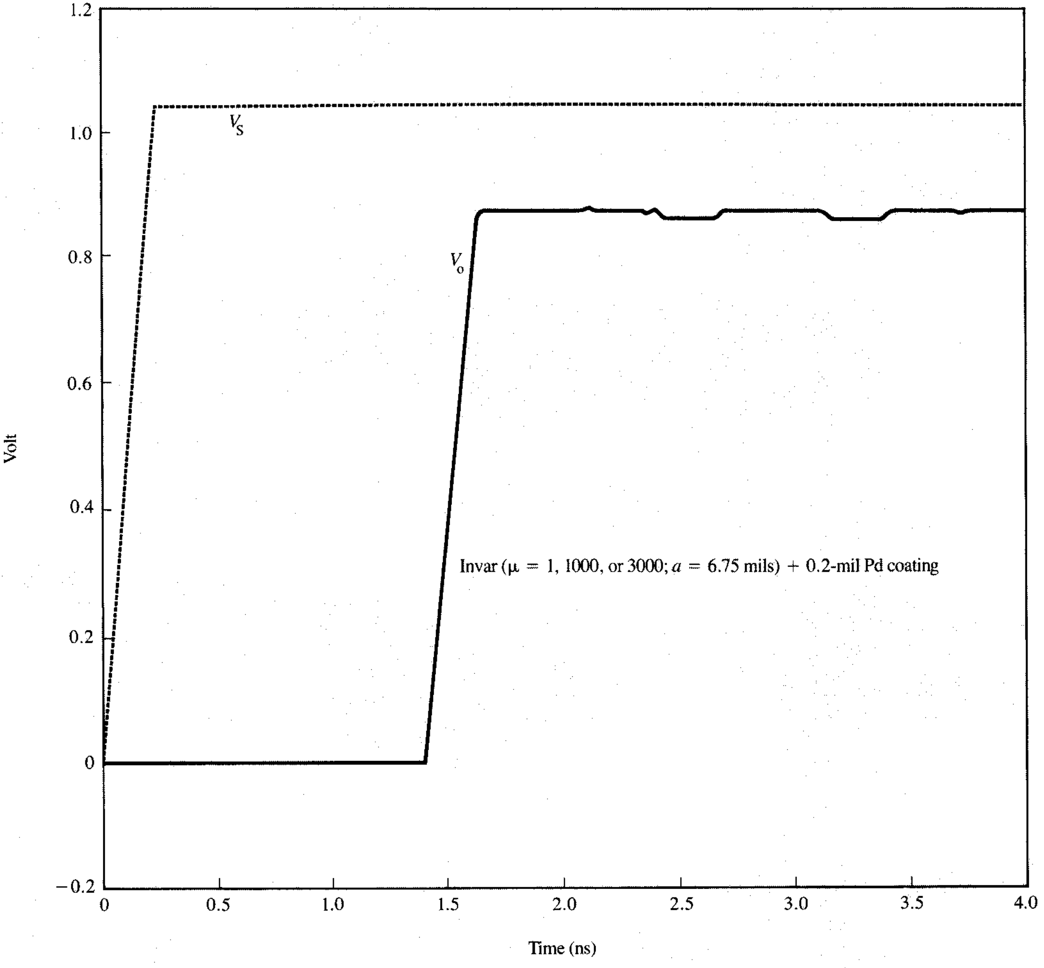

Figure 9

Time response of V_o where the Invar pins (a = 6.75 mils) are coated with 0.2 mil of Pd. No difference is observed whether μ/μ_o = 1, 1000, or 3000 for Invar.

Acknowledgment

Thanks are due to M. Potter for providing information on the module pins. B. J. Rubin's careful review of the manuscript is also appreciated.

Appendix A: Matrix of $[A]_{10\times 10}$

The boundary conditions in Figure 2 require that the voltage and current be continuous at the interfaces (a) between the source and transmission line 1, (b) between transmission lines, and (c) between transmission line 5 and the load. That is,

$$V_S = I_1(0)R_S + V_1(0), \tag{A1}$$

$$V_i(\ell_i) = V_{i+1}(0), \tag{A2}$$

$$I_i(\ell_i) = I_{i+1}(0), \tag{A3}$$

$$V_5(\ell_5) = I_5(\ell_5)R_L, \tag{A4}$$

where $1 \leqq i \leqq 4$.

In matrix form, one has

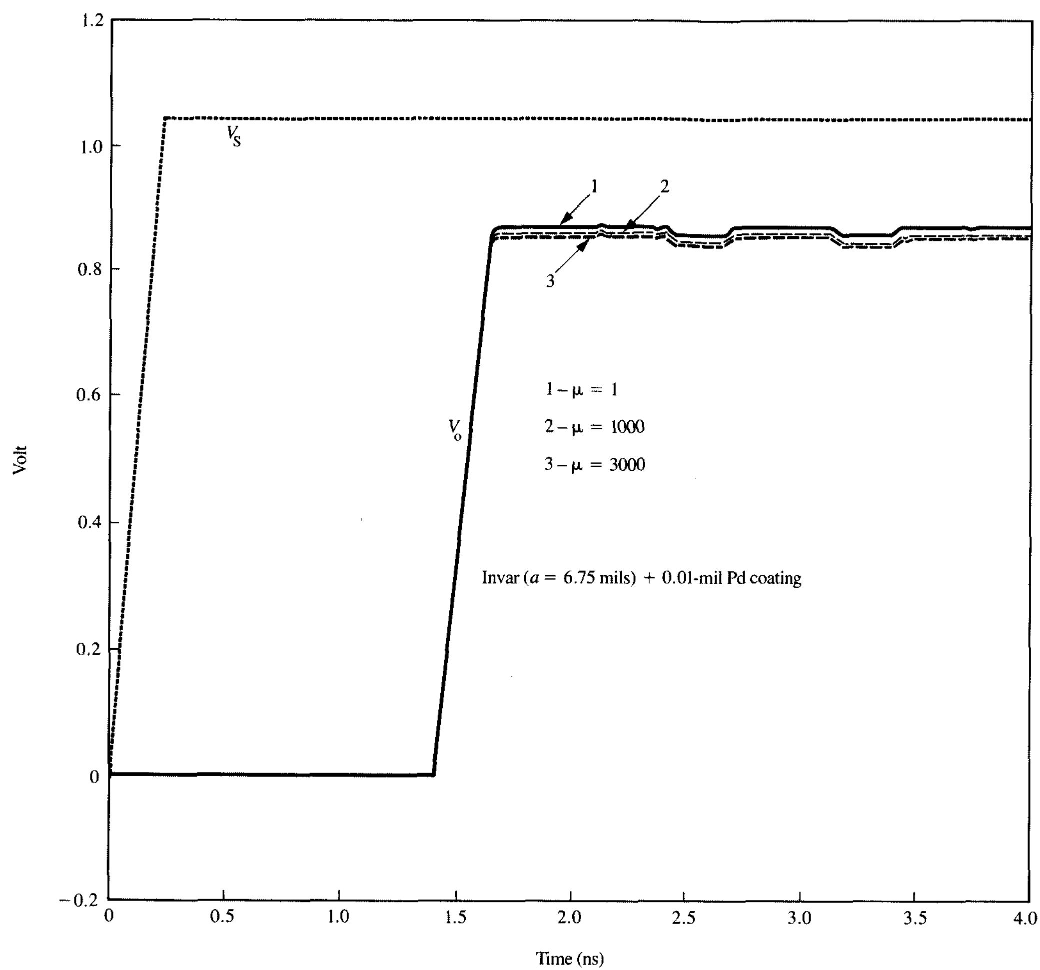

Figure 10

Time response of V_o where the Invar pins (a = 6.75 mils) are coated with 0.01 mil of Pd. More signal degradation is observed when Invar has a higher μ.

$$\begin{bmatrix} 1 + Y_{c1}R_S & 1 - Y_{c1}R_S & 0 & 0 & & 0 & 0 \\ e^{-\gamma_1 l_1} & e^{+\gamma_1 l_1} & -1 & -1 & & 0 & 0 \\ Y_{c1}e^{-\gamma_1 l_1} & -Y_{c1}e^{+\gamma_1 l_1} & -Y_{c2} & +Y_{c2} & & 0 & 0 \\ 0 & 0 & e^{-\gamma_2 l_2} & e^{+\gamma_2 l_2} & & 0 & 0 \\ 0 & 0 & Y_{c2}e^{-\gamma_2 l_2} & -Y_{c2}e^{+\gamma_2 l_2} & \cdots & 0 & 0 \\ 0 & 0 & 0 & 0 & & 0 & 0 \\ 0 & 0 & 0 & 0 & & 0 & 0 \\ 0 & 0 & 0 & 0 & & -1 & -1 \\ 0 & 0 & 0 & 0 & & -Y_{c5} & +Y_{c5} \\ 0 & 0 & 0 & 0 & & e^{-\gamma_5 l_5}(1 - Y_{c5}R_L) & e^{+\gamma_5 l_5}(1 + Y_{c5}R_L) \end{bmatrix} \begin{bmatrix} V_1^+ \\ V_1^- \\ V_2^+ \\ V_2^- \\ V_3^+ \\ V_3^- \\ V_4^+ \\ V_4^- \\ V_5^+ \\ V_5^- \end{bmatrix} = \begin{bmatrix} V_S \\ 0 \\ 0 \\ 0 \\ 0 \\ 0 \\ 0 \\ 0 \\ 0 \\ 0 \end{bmatrix}$$

Appendix B: Reduction of Equation (17)

Equation (17) can be reduced to Equation (18) through the following. Let $[\tilde{Y}] = [\tilde{Z}]^{-1}$; then

$$[\tilde{I}] = [\tilde{Y}]_{(N+1)\times(N+1)} [\tilde{V}_{Q}]. \tag{B1}$$

Adding the columns and rows of $[\tilde{Y}]$ $(= [\tilde{Y}_{ij}])$, one has

$$\begin{bmatrix} \tilde{I}_{S} \\ \sum_{n=1}^{N} \tilde{I}_{n} \end{bmatrix} = \begin{bmatrix} \tilde{Y}_{11} & \sum_{j=2}^{N+1} \tilde{Y}_{ij} \\ \sum_{i=2}^{N+1} \tilde{Y}_{i1} & \sum_{i=2}^{N+1} \sum_{j=2}^{N+1} \tilde{Y}_{ij} \end{bmatrix} \begin{bmatrix} \tilde{V}_{S} \\ \tilde{V} \end{bmatrix}. \tag{B2}$$

References

1. *Alloy Digest*, Engineering Alloys Digest, Inc., Upper Montclair, NJ, August and October 1953.
2. R. E. Collin, *Foundations for Microwave Engineering*, McGraw-Hill Book Co., Inc., New York, 1966.
3. J. A. Stratton, *Electromagnetic Theory*, McGraw-Hill Book Co., Inc., New York, 1941.
4. F. Grover, *Inductance Calculations: Working Formulas and Tables*, Dover Publications, New York, 1962.
5. E. E. Davidson, "Electrical Design of a High Speed Computer Package," *IBM J. Res. Develop.* **26,** No. 3, 349–361 (May 1982).

Received November 5, 1986; accepted for publication March 24, 1987

Ching-Chao Huang *IBM General Technology Division, East Fishkill facility, Route 52, Hopewell Junction, New York 12533.* Dr. Huang received the B.S. degree from the National Taiwan University, Taipei, Taiwan, in 1976, and the M.S. and Ph.D. degrees, all in electrical engineering, from Ohio State University, Columbus, Ohio, in 1980 and 1982, respectively. He joined IBM in 1983, and is currently an advisory engineer. His research interests include VLSI package modeling, inductance and capacitance calculation, numerical techniques in electromagnetics, and diffraction theory. Dr. Huang is a member of the Institute of Electrical and Electronics Engineers.

Leon Li-Heng Wu *IBM General Technology Division, East Fishkill facility, Route 52, Hopewell Junction, New York 12533.* Dr. Wu is a senior engineer working on advanced package modeling and design. After joining IBM in 1968, he worked on diffusion profile modeling, silicon defect studies, device modeling, and thermal printer design. In 1962, he received his B.S. in electrical engineering from the National Taiwan University, Taipei, Taiwan. Dr. Wu received his M.S. in 1965 and his Ph.D. in 1968, both in electrical engineering, from Carnegie-Mellon University, Pittsburgh, Pennsylvania.